Singularity structure of the πN scattering amplitude in a meson-exchange model up to energies $W \leq 2.0$ GeV

L. Tiator[a], S.S. Kamalov[a,b,d], S. Ceci[c], Guan Yeu Chen[d], D. Drechsel[a], A. Svarc[c], and Shin Nan Yang[d]

[a]Institut für Kernphyik, Universität Mainz, D-55099 Mainz, Germany

[b]Bogoliubov Laboratory for Theoretical Physics, JINR, Dubna, 141980 Moscow Region, Russia

[c]Rudjer Boskovic Institute, Division of Experimental Physics, HR-10002 Zagreb, Croatia

[d]Department of Physics and Center for Theoretical Sciences, National Taiwan University, Taipei 10617, Taiwan

(Dated: October 11, 2010)

Within the previously developed Dubna-Mainz-Taipei meson-exchange model, the singularity structure of the πN scattering amplitudes has been investigated. For all partial waves up to F waves and c.m. energies up to $W \sim 2$ GeV, the T-matrix poles have been calculated by three different techniques: analytic continuation into the complex energy plane, speed-plot, and regularization method. For all 4-star resonances except the $S_{11}(1535)$, we find very good agreement between the analytic continuation and the regularization method. We also find resonance poles for resonances that are not so well established, but in these cases the pole positions and residues obtained by analytic continuation can substantially differ from the results predicted by the speed-plot and regularization methods.

PACS numbers: 11.80.Gw, 13.75.Gx, 14.20.Gk, 25.80.Dj
Keywords: pion-nucleon interaction, baryon resonances, T-matrix poles, speed plot, regularization method

I. INTRODUCTION

Ever since the $\Delta(1232)$ resonance was discovered by Fermi and collaborators in 1952 [1–3], the excitation spectrum of the nucleon has played a fundamental role in our understanding of low-energy hadronic physics. The most direct evidence for resonance structure is based on pion-nucleon elastic and charge-exchange scattering. Because total angular momentum, parity, and isospin are conserved within the realm of the strong interaction, the S matrix for the reactions $\pi + N \rightarrow \pi' + N'$ may be decomposed into the partial wave amplitudes $T^I_{\ell\pm}$, with I the isospin, ℓ the orbital angular momentum, and the $\pm$ indicating the total spin of the hadronic system, $J = \ell \pm \frac{1}{2}$. Two decades after the discovery of the $\Delta(1232)$, a dedicated program at the meson factories had provided enough data to establish a rich resonance spectrum of the nucleon [4, 5]. The further partial wave analysis was driven by studies of the Karlsruhe-Helsinki (KH) [6, 7] and Carnegie-Mellon–Berkeley (CMB) [8, 9] collaborations. In the following years, R. Arndt and coworkers at VPI compiled the data base SAID [10], which was later updated and extended in collaboration with GWU [11, 12]. The works of the CMB, KH, and GW/VPI groups are the main sources of the nucleon resonance listings in the Review of Particle Physics (PDG) [13].

In the most intuitive way, a resonance is an intermediate state of target and projectile that lives longer than in a typical scattering process. Translated into the language of scattering theory, resonances are defined as poles of the S matrix. Different methods were developed to derive the resonance properties from the observables. In the 1930's it was suggested that a Breit-Wigner function should be a good representation for a resonance pole, and the Breit-Wigner formula for spin zero particles and its generalization to finite spin were developed (see an illustrative discussion in Cottingham and Greenwood, p. 241 in Ref. [14]). Later the discussion centered on the rapid increase of the eigenphase shifts through 90° and on the related backward looping of Argand diagrams [15].

However, Breit-Wigner parametrizations have been found to be very model dependent. As was recently shown in the framework of effective quantum field theory, Breit-Wigner masses are in general field-redefinition dependent [16]. The same model dependency also applies to electromagnetic properties as charges, magnetic moments, transition moments, and form factors. On the other side, all these resonance properties are uniquely defined at the pole of the S matrix [17].

The analytic properties of the S matrix are imposed by the principles of unitarity and causality. Because of unitarity, each physical channel leads to a square-root type branch point of the partial wave amplitude $T(W)$ at the respective threshold, with the result that $T(W)$ is a multi-valued function in the complex W plane. In particular, if the branch cut is taken on the real axis to the right, a partial wave for elastic πN scattering is described by the amplitudes $T^{[1]}$ on the physical and $T^{[2]}$ on the unphysical sheet. The experimental amplitudes are identified with the amplitudes above the cut, $T_{\rm exp}(W) = \lim_{\epsilon\to 0} T^{[1]}(W + i\,\epsilon)$, with $W > M + m$ and $\epsilon > 0$. As a consequence, the physical sheet has a discontinuity over the real axis, along the right-hand cut $M + m \leq W < \infty$, with M the nucleon and m the pion mass. Causality requires that the physical sheet be free of any further singularity, the nucleon resonances should appear as simple poles on the unphysical sheet closest to the real axis of the physical sheet, in agreement with Höhler's remark [18]: *"It is 'noncontroversial among theorists' (see Chew [19] and the references in my 'pole-emics', p.697 in Ref. [20]) that in S-matrix theory the effects of resonances follow from first order poles in the 2nd sheet."* A pole on the second sheet, described by $T^{[2]}(W) \approx r_p/(M_p - W - i\,\Gamma_p/2)$, will often lead to a maximum of the experimental cross section near $W = M_p$. The resonance is therefore defined by (i) its pole position in the complex c.m. energy plane at $W_p = M_p - i\,\Gamma_p/2$, with M_p the real part of the pole position and Γ_p the width of the resonance, and (ii) the residue of the amplitude, $r_p = |r_p|\exp(i\,\theta_p)$, at the pole.

In a more physical way, resonance is characterized by a maximum time delay, the time passing between the arrival of a wave packet and its departure from the collision region. In general, a large time delay indicates the formation of an unstable particle in the intermediate state. However, misleading effects can occur by rapid variation of backgrounds, such as narrow cusp effects above S-wave thresholds or spurious singularities due to phenomenological parametrization of form factors and cut-offs. If a resonance lives long enough, it should decay into all energetically possible final states, unless prevented by general selection rules. Furthermore, the pole position derived from the data should not depend on how the resonance is excited or decays. Whereas such resonances exist in atomic and also in nuclear physics, some caveat is in order for nucleon resonances. As an example, a simple classical model of the $\Delta(1232)$ leads to the conclusion that the pion stays in its orbit around the nucleon for only about 100° of a full circle.

The focus of the present work is on how to extract resonance properties from the data, that is, how do we find a pole in the complex energy plane having at our disposal only data on the real axis. Different pole-extraction methods have been applied in the past. The pole positions of nucleon resonances have often been derived from the data by the speed plot [4, 21], which is related to the time delay. The "speed" is defined by the slope of the amplitude with energy, $dT(W)/dW$, which eliminates constant backgrounds. The "speed plot" (SP) shows the modulus of the speed, $\mathrm{SP}(W) = |dT(W)/dW|$, and resonances are identified with peaks in the plot. The resonance parameters are then obtained by fitting the speed of a single pole to the data at physical values of the energy. The idea of the speed plot has been recently generalized to higher derivatives by the "regularization method" (RM) [22]. Within a convergence circle given by the closest neighboring singularity, the Laurent expansion about a pole is given by the sum of $T^{\rm pole}(W)$ and a Taylor series $T^{\rm reg}(W)$. With an increasing number of differentiations, the signature of the pole sticks out more and more sharply, whereas more and more leading terms of the Taylor series disappear. It

goes without saying that the differentiation of the data will fail after a few steps because of numerical instabilities. However, the regularization method is an interesting tool to study the singularity structure of analytic models. In particular, this method will reveal any rapid variation due to cusp effects and spurious singularities introduced by phenomenological parameterizations.

Although Lattice QCD (LQCD) has obtained promising results for the masses and several resonances of the low-lying hadrons [23–25], the large pion mass used and the quenching approximation make it (yet) impossible to treat the resonances as a pion-nucleon scattering state. As shown by Ref. [26] for the $N\Delta$ form factors, the chiral extrapolation from the stable Δ at large pion masses to the experimental pion mass yields unexpected and rather dramatic non-analytic effects at the $\Delta \to N\pi$ threshold. The very fact that lattice theory can not yet describe the pion-nucleon final state interaction, makes it impossible to compare the lattice data to the experimental scattering amplitudes in a direct way. In principle, the LQCD data should be compared to the results of effective field theories or dynamical models which are extrapolated to the pion mass used in LQCD. In addition to kinematical mass effects such as shifts of branch points also the mass dependence of the coupling constants should be considered. As long as the pion mass is large, $m_\pi > m_{N^*} - m_N$, the N* appears as an excited bound state. In this case the mass predicted by LQCD should be compared to the "dressed" mass of the dynamical model, which contains the "bare" mass and a real self-energy due to meson loops. In the mass region where the N* decays, the LQCD calculation would provide a complex amplitude, comparable to the scattering phases of a partial wave expansion. Based on the work of Lüscher [27], the width of the rho meson [28] and of the Delta resonance [29] have been recently studied. In such a case the lattice data can be treated like experimental amplitudes, that is, by speed plot or Breit-Wigner analyses. However, as long as the LQCD pion mass lies above the physical value, an extrapolation to the physical pion mass will still be necessary by use of a dynamical model or an effective field theory.

In the present contribution we study the Dubna-Mainz-Taipei model (DMT) [30] by comparing the pole parameters resulting from analytic continuation with approximate procedures such as the speed plot and the regularization method. The DMT is similar in spirit with the work of several other collaborations [30–36] who have studied the nucleon resonances within Lagrangian models. The building blocks of these models are "bare" resonances simulating quark configurations which are "dressed" by meson-nucleon continua through the respective Lagrangians. Compared to the partial wave amplitudes obtained in Refs. [8–12], the dynamical models provide a field-theoretical description of pion-nucleon scattering by meson-baryon loops. Therefore, the energy dependence of the DMT amplitudes is largely determined by theoretical considerations even though there are free parameters in the model. Another strong point of the DMT is the fact that its predictions for electromagnetic pion production [37–39] are in excellent agreement with the experimental data from threshold up to the $\Delta(1232)$ region. In Sect. II we give an overview of the speed-plot, time-delay, and regularization methods to derive the pole parameters. The Dubna-Mainz-Taipei model is presented in Sect. III, in particular with regard to the definitions of resonant vs. background terms as well as form factors and cut-offs. Our results for the resonance parameters are reported in Sect. IV, and the different techniques to derive these parameters are compared. We conclude with a summary and outlook in Sect. V.

II. HOW TO FIND A RESONANCE

A. Time delay

In the framework of a potential scattering problem, resonance phenomena are related to the formation and the decay of intermediate quasi-stationary states. A resonance should decay in all energetically possible final states, unless forbidden by selection rules for a specific channel. Provided that the interaction is of short range, resonances can be characterized by the *time delay* between the arrival of a wave packet and its departure from the collision region. In general, the time delay shows a pronounced peak at the resonance energies. The time delay was introduced by Eisenbud in his Ph.D. thesis [40] and later applied to multi-channel scattering theory by Smith [41]. Following the work of Refs. [15, 42–44], we define the time delay for a single-channel scattering problem in a partial wave as follows:

$$\Delta t(W) = \mathrm{Re}\left(-i\frac{1}{S(W)}\frac{dS(W)}{dW}\right) = 2\,\frac{d\delta(W)}{dW}\,, \tag{1}$$

where $S(W) = \exp[2i\delta(W)]$ is the S matrix and $\delta(W)$ the scattering phase shift. A simple ansatz for a unitary S matrix with a pole at $W_p = M_p - \frac{i}{2}\Gamma_p$ and a constant background phase δ_B is given by

$$S(W) = \frac{M_p + \frac{i}{2}\Gamma_p - W}{M_p - \frac{i}{2}\Gamma_p - W}\,e^{2i\delta_B} = e^{2i\delta_R(W)}\,e^{2i\delta_B}\,, \tag{2}$$

where $\delta_R(W) = \arctan[\frac{1}{2}\Gamma_p/(M_p - W)]$ is the resonant phase. The related T-matrix $T = (S-1)/(2\,i)$ and the real matrix $K = i\,(1-S)(1+S)^{-1}$ take the forms

$$T(W) \;=\; \frac{\frac{1}{2}\Gamma_p}{M_p - \frac{i}{2}\Gamma_p - W}\,e^{2i\delta_B} + \sin\delta_B e^{i\delta_B}\,, \tag{3}$$

$$K(W) \;=\; \frac{\frac{1}{2}\Gamma_p + (M_p - W)\tan\delta_B}{M_p - W - \frac{1}{2}\Gamma_p\tan\delta_B}\,. \tag{4}$$

Combining Eqs. (1) and (2), we obtain a simple form for the time delay,

$$\Delta t(W) = \frac{\Gamma_p}{(W - M_p)^2 + \frac{1}{4}\Gamma_p^2}\,. \tag{5}$$

In this ideal case, the maximum time delay is $\Delta t(M_p) = 4/\Gamma_p$. We observe that both the real (M_p) and imaginary ($-\frac{1}{2}\Gamma_p$) parts of the pole position are determined by the time delay (and therefore also by the scattering matrix) at real (physical!) values of the c.m. energy W.

In order to describe a system of coupled channels, the lifetime matrix Q was introduced [41],

$$Q_{ij}(W) = -i\frac{dS_{ik}(W)}{dW}\,S^*_{jk}(W)\,. \tag{6}$$

The analog of the time delay for a multi-channel system was found to be the trace of Q as function of W. This trace takes a more transparent form after diagonalization of the S matrix [15, 45],

$$\mathrm{tr}[Q(W)] = 2\sum_\alpha \frac{d\delta_\alpha(W)}{dW}\,, \tag{7}$$

with δ_α the eigenphase shifts. However, a realistic application of the lifetime matrix requires the knowledge of all open channels, that is, the reactions $\pi N \to \pi N$, $\pi N \to \pi\pi N$, $\pi\pi N \to \pi\pi N$, $\pi N \to \eta N$, and so on. As a consequence of the Neumann-Wigner no-crossing theorem [46], individual eigenphases have a complicated energy dependence. It

is therefore only the sum of the eigenphases that shows distinct resonance structures. Based on this observation, it has been recently proposed to search for resonance parameters by studying the traces of multi-channel T and K matrices [47, 48]. The respective scattering matrices were constructed from experimental data for the πN and ηN channels and models for the two-pion channels.

B. Speed plot

The *speed plot* of a partial wave amplitude T is defined by

$$\mathrm{SP}(W) = \left| \frac{dT(W)}{dW} \right| . \tag{8}$$

As was recognized by the Particle Data Group already in the early 1970's, the speed plot is a convenient tool to extract the pole position of a resonance [5, 49]. This technique was intensively studied by Höhler who wanted to extract resonance parameters from the Karlsruhe-Helsinki partial wave analysis (KH80) [21, 50]. Because the KH analysis was restricted to elastic pion-nucleon scattering, a multi-channel treatment like the construction of the lifetime matrix was out of reach.

For a single channel system, the time delay and the speed plot are identical up to a factor 2. In particular, the pole ansatz of Eq. (3) leads to the speed

$$\mathrm{SP}(W) = \frac{\frac{1}{2}\Gamma_p}{(W - M_p)^2 + \frac{1}{4}\Gamma_p^2} . \tag{9}$$

As a result, the speed plot shows a maximum for $W = M_p$, which defines the real part of the pole position in the complex W plane. The imaginary part of the pole position can be obtained from the relation

$$\mathrm{SP}(M_p \pm \tfrac{1}{2}\Gamma_p) = \tfrac{1}{2}\,\mathrm{SP}(M_p) . \tag{10}$$

In practical applications, this straightforward method has to be modified. In the vicinity of a pole, Eq. (3) can be generalized to

$$T(W) = \frac{r_p}{M_p - W - \frac{i}{2}\,\Gamma_p} \; + \; T^{\mathrm{reg}}(W) \tag{11}$$

with T^{reg} a regular function of the energy W and r_p, the complex residue at the pole, given by

$$\mathrm{Res}\, T(W)|_{W=W_p} = - \mid r_p \mid \; e^{i\theta_p} . \tag{12}$$

If all higher-order terms are neglected, Eq. (8) leads to the more general speed

$$\mathrm{SP}(W) = \frac{|r_p|}{(W - M_p)^2 + \frac{1}{4}\Gamma_p^2} , \tag{13}$$

which is fitted to speed data obtained from the partial wave amplitudes in the vicinity of the maximum. The pole parameters M_p, Γ_p and $|r_p|$ are then obtained from the best fit to the selected speed points. Finally, the phase θ_p of the residue is obtained from the phase of dT/dW,

$$\theta_p = \arg\left(-\frac{dT}{dW}\bigg|_{W=M_p} \right) . \tag{14}$$

C. Regularization method

As discussed before, the speed plot technique is successful if the background under the resonance is approximately constant. It fails if the background changes over the resonance region. The *regularization method* extends the idea behind the speed plot by construction of higher derivatives, $T^{(N)} \equiv d^N\,T/dT^N$, $N \geq 1$ [22]. Let there be an analytic function $T(z)$ of a complex variable z with a first-order pole at some complex point $\mu = x + iy$. This function can be any of the T-matrix elements, and the variable z is identified with the c.m. energy W in order to compare with the speed plot technique. The described function takes the form

$$T(z) = \underbrace{\frac{r}{\mu - z}}_{\text{pole part}} + \underbrace{\left(T(z) - \frac{r}{\mu - z}\right)}_{\text{non-pole part}}, \tag{15}$$

where μ and r are the position and residue of the pole. In a sufficiently small region around the pole, the non-pole part is a smooth analytical function. Of course, the experiment can determine the T-matrix elements only for real values of W. In order to continue $T(W)$ into the complex energy plane and to search for the pole position, we construct a regular function f by multiplying T with the factor $\mu - z$,

$$f(z) = (\mu - z)\,T(z)\,, \tag{16}$$

with $f(\mu) = r$. In the neighborhood of the pole, the function f can be expanded in a Taylor series. Because the scattering matrix can be accessed for real arguments only, we construct $f(\mu)$ from the derivatives of f taken along the real axis,

$$r = f(\mu) = \sum_{n=0}^{N} \frac{f^{(n)}(W)}{n!}(\mu - W)^n + R_N(W, \mu). \tag{17}$$

This expansion is explicitly written to order N, and $R_N(W, \mu)$ stands for the higher orders. The derivatives $f^{(n)}(W)$ can be turned in derivatives of the T matrix by use of Eq. (16), and mathematical induction leads to the following equation:

$$f^{(n)}(W) = (\mu - W)\,T^{(n)}(W) - n\;T^{(n-1)}(W). \tag{18}$$

Insertion of these derivatives into Eq. (16) cancels all the terms in the sum except for the last one,

$$r = \frac{T^{(N)}(W)}{N!}(\mu - W)^{(N+1)} + R_N(W, \mu)\,. \tag{19}$$

In the neighborhood of the pole, the remainder R_N should decrease with increasing N. Assuming that the higher derivatives can be neglected for a sufficiently large value of N and taking the absolute values of both sides, we obtain an approximation of the pole parameters at $\mathcal{O}(N)$,

$$|r_N| = \frac{\left|T^{(N)}(W)\right|}{N!}\,|\mu_N - W|^{(N+1)}\,. \tag{20}$$

On condition that the Taylor series converges and in the limit $N \to \infty$, r_N and μ_N should approach the values r and μ, respectively. In the next step, we (i) write the pole position as a general complex number, $\mu = a + i\,b$, (ii) raise both sides of Eq. (20) to the power of $2/(N+1)$, and collect the information about the T-matrix and the pole position on the right and left side, respectively. The result is a parabolic equation in W,

$$\frac{(a_N - W)^2 + b_N^2}{\sqrt[N+1]{|r_N|^2}} = \sqrt[N+1]{\frac{(N!)^2}{\left|T^{(N)}(W)\right|^2}}\,. \tag{21}$$

This equation relates the pole position ($a = M_p$, $b = -\frac{1}{2}\,\Gamma_p$) and the absolute value of the residue, $|r|$, to the T-matrix values on the real axis, as obtained from a model or an energy-dependent partial-wave analysis of the data. Finally, the phase of the residue is determined by

$$\theta_N = \arg\Big(\,(-i)^{N+1}\;T^{(N)}(M_p)\,\Big)\;. \tag{22}$$

The comparison of the above equations with the results of Sect. II B shows that the speed plot is identical to the regularization method for $N = 1$.

The further procedure is as follows: (i) Construct the N^{th} derivative of the T-matrix element and the right-hand side of Eq. (21). Note that the pole parameters are uniquely determined by the *exact* knowledge of $T(W)$ in only *three points*. However, the problem is to choose the right points. If the distance between the points gets too large, the influence of other singularities may increase. If the points are too close, numerical problems may occur. (ii) Solve Eq. (21) for the pole parameters by either choosing various three-point sets to evaluate the right-hand side and perform a statistic analysis of the results or fitting the right-hand side of the equation to a three-parameter parabolic function. In our approach we have chosen the latter option.

In closing this section we note that the regularization method does not depend on any particular functional form of the T matrix. However, we have to assume that (a) the N^{th} derivative can be constructed with a sufficient precision and (b) the pole position lies within the circle of convergence for the Taylor expansion, that is, no further singularities should intrude into the region between the pole and the related resonance region on the real W axis.

D. Poles from analytic continuation

The most accurate way to determine pole positions and residues is certainly obtained by analytic continuation into the complex region. Because resonance poles can not appear on the physical sheet, we have to take a careful look at the structure of different Riemann sheets opening at all branch points for particle production in a coupled-channels model. The most important particle thresholds in our energy region below 2 GeV are $\pi\pi N$, $\pi\Delta$, ηN, and ρN with branch points at 1178 MeV, $(1350 - 50i)$ MeV, 1486 MeV, and $(1713 - 75i)$ MeV, in order. In the dynamical DMT model we have included the πN and $\pi\pi N$ channels in all the partial waves and the ηN channel in the S_{11} partial wave. However, the $\pi\pi N$ channel is treated in a phenomenological way as will be described in the following section. Because the particular ansatz for the two-pion width, Eq. (36), contains only even powers of $q_{2\pi}$, the model does not give additional branch points for the two-pion channel. This leads to a relatively simple sheet structure, and we can easily reach the poles on the most important second Riemann sheet (first unphysical sheet). Technically, we first map the relevant region on this sheet by contour plots and search for the accurate pole position by standard root finding routines applied to the function

$$h(z_p) = \frac{1}{|T(z_p)|} = 0\,. \tag{23}$$

Next we obtain the residue by approaching the pole along different paths in the complex plane,

$$\mathrm{Res}\,T(z)|_{z_p} = \lim_{z\to z_p}(z - z_p)\,T(z)\,. \tag{24}$$

A word of caution is in order. If the fitted form factor parameters, e.g., Λ_α of Eq. (32) or X_R of Eq. (36) become smaller than about 500 MeV, additional poles can appear in the region where the resonance poles are expected. In

order to avoid such spurious singularities, it is very important to map out the structure of the T matrix very precisely. Also the speed-plot and regularization methods are very helpful to distinguish between resonance and spurious poles, because the latter ones usually affect the T matrix at real W in a similar way as a broad background does.

III. THE DUBNA-MAINZ-TAIPEI MESON-EXCHANGE MODEL

The Dubna-Mainz-Taipei (DMT) πN meson-exchange model was developed on the basis of the Taipei-Argonne πN meson-exchange model [51–53] which describes pion-nucleon scattering up to 400 MeV pion laboratory energy. The DMT πN model was extended to c.m. energies $W = 2.0$ GeV by inclusion of higher resonances and the ηN channel [30, 54]. The model describes well both πN phase shifts and inelasticity parameters in all the channels up to the F waves and energies of 2 GeV [55], except for the F_{17} partial wave. The DMT πN model is also a main ingredient of the DMT dynamical model describing the photo- and electroproduction of pions [56] up to 2 GeV. This model gives an excellent agreement with pion production data from threshold to the first resonance region [37, 57]. In this section, we briefly outline the ingredients of the Taipei-Argonne πN model and then describe some relevant features of the DMT meson-exchange coupled-channels model. For more details, we refer readers to [30, 53, 54].

A. Taipei-Argonne meson-exchange πN model

The Taipei-Argonne model describes the elastic scattering of pions and nucleons. It is based on a three-dimensional reduction of the Bethe-Salpeter equation for an effective Lagrangian involving π, N, Δ, ρ, and σ fields. Let us consider the πN scattering,

$$\pi(q) + N(p) \to \pi(q') + N(p') \,, \tag{25}$$

where q, p, q', and p' are the four-momenta of the respective particles. The total and relative four-momenta are $P = p + q$ and $k = p\,\eta_\pi(s) - q\,\eta_N(s)$, respectively, where $s = P^2 = W^2$. The dimensionless variables $\eta_\pi(s)$ and $\eta_N(s)$ represent a freedom in choosing a three-dimensional reduction, and are constrained by $\eta_N + \eta_\pi = 1$.

The Bethe-Salpeter equation for πN scattering takes the form

$$T_{\pi N} = B_{\pi N} + B_{\pi N} G_0 T_{\pi N} \,, \tag{26}$$

where $B_{\pi N}$ is the sum of all irreducible two-particle Feynman amplitudes and G_0 the free relativistic πN propagator. Eq. (26) can be cast into the form

$$T_{\pi N} = \hat{B}_{\pi N} + \hat{B}_{\pi N} \hat{G}_0 T_{\pi N} \,, \tag{27}$$

with

$$\hat{B}_{\pi N} = B_{\pi N} + B_{\pi N} (G_0 - \hat{G}_0) \hat{B}_{\pi N} \,, \tag{28}$$

where $\hat{G}_0(k; P)$ is an appropriate propagator to obtain a three-dimensional reduction of Eq. (26). This propagator is typically chosen to maintain the two-body unitarity by reproducing the πN elastic cut. However, there is still a wide range of possible propagators satisfying this constraint. We chose the Cooper-Jennings propagator [58] since it can satisfy the soft-pion theorems. It takes the following form in the c.m. frame:

$$\hat{G}_0(k; s) = \frac{1}{(2\pi)^3} \frac{\delta[k_0 - \hat{\eta}(s_{\vec{k}}, \vec{k})]}{\sqrt{s} - \sqrt{s_{\vec{k}}}} \frac{2\sqrt{s_{\vec{k}}}}{\sqrt{s} + \sqrt{s_{\vec{k}}}} f(s, s_{\vec{k}}) \frac{\eta_N(s) \gamma_0 \sqrt{s} + \not{k} + m_N}{4 E_N(\vec{k}) E_\pi(\vec{k})} \,, \tag{29}$$

where $E_N(\vec{k})$ and $E_\pi(\vec{k})$ are the nucleon and pion energies for three-momentum $\vec{k}$; $\sqrt{s_{\vec{k}}} = E_N(\vec{k}) + E_\pi(\vec{k})$ is the total c.m. energy, and $\hat{\eta}(s,\vec{k}) = E_N(\vec{k}) - \eta_N(s_{\vec{k}})\sqrt{s_{\vec{k}}}$, with $\eta_N(s) = (s + m_N^2 - m_\pi^2)/2s$. With these relations we obtain the following πN scattering equation:

$$t(\vec{k'},\vec{k};W) = v(\vec{k'},\vec{k};W) + \int d\vec{k''} v(\vec{k'},\vec{k''};W) g_0(\vec{k''};W) t(\vec{k''},\vec{k};W)\,, \tag{30}$$

where t and v are related to $T(k',k;P)$ and $B(k',k;P)$ by setting $k'_0 = \hat{\eta}(s_{\vec{k'}},\vec{k'})$ and $k_0 = \hat{\eta}(s_{\vec{k}},\vec{k})$, while g is obtained from G with $k_0 = 0$.

The effective Lagrangian involving the π, N, σ, ρ, and $\Delta(1232)$ fields takes the form

$$\begin{aligned}
\mathcal{L}_I \;=\; & \frac{f^{(0)}_{\pi NN}}{m_\pi}\bar{N}\gamma_5\gamma_\mu\vec{\tau}\cdot\partial^\mu\vec{\pi}N - g^{(s)}_{\sigma\pi\pi}m_\pi\sigma(\vec{\pi}\cdot\vec{\pi}) - \frac{g^{(v)}_{\sigma\pi\pi}}{2m_\pi}\sigma(\partial^\mu\vec{\pi}\cdot\partial_\mu\vec{\pi}) - g_{\sigma NN}\bar{N}\sigma N \\
& - g_{\rho NN}\bar{N}\{\gamma_\mu\vec{\rho}^{\,\mu} + \frac{\kappa^\rho_V}{4m_N}\sigma_{\mu\nu}(\partial^\mu\vec{\rho}^{\,\nu} - \partial^\nu\vec{\rho}^{\,\mu})\}\cdot\frac{1}{2}\vec{\tau}N \\
& - g_{\rho\pi\pi}\vec{\rho}^{\,\mu}\cdot(\vec{\pi}\times\partial_\mu\vec{\pi}) - \frac{g_{\rho\pi\pi}}{4m_\rho^2}(\delta-1)(\partial^\mu\vec{\rho}^{\,\nu} - \partial^\nu\vec{\rho}^{\,\mu})\cdot(\partial_\mu\vec{\pi}\times\partial_\nu\vec{\pi}) \\
& + \frac{g_{\pi N\Delta}}{m_\pi}\bar{\Delta}_\mu[g^{\mu\nu} - (Z+\frac{1}{2})\gamma^\mu\gamma^\nu]\vec{T}_{\Delta N}N\cdot\partial_\nu\vec{\pi}\,,
\end{aligned} \tag{31}$$

with Δ_μ the Δ field operator and $\vec{T}_{\Delta N}$ the isospin transition operator between nucleon and Δ. The pseudovector πNN coupling is dictated by the chiral symmetry.

The driving term $B_{\pi N}$ in Eq. (26) is approximated by the tree diagrams of the interaction Lagrangian of Eq. (31), containing direct and crossed N and Δ diagrams as well as the t-channel σ- and ρ-exchange contributions.

Furthermore, the driving term $v(\vec{k},\vec{k'};W)$ of Eq. (30) is regularized by covariant form factors associated with each leg α of the vertices,

$$F_\alpha(p_\alpha^2) = \left[\frac{n\Lambda_\alpha^4}{n\Lambda_\alpha^4 + (m_\alpha^2 - p_\alpha^2)^2}\right]^n\,, \tag{32}$$

with p_α the four-momentum and m_α the mass of particle α. $n = 10$ was used in Ref. [54].

As in [59, 60], the P_{11} phase shift is constrained by imposing the nucleon pole condition. This treatment leads to a proper renormalization of both nucleon mass and πNN coupling constant. It also yields the necessary cancelation between the repulsive nucleon pole contribution and the attractive background, such that a reasonable fit to the πN phase shifts in the P_{11} channel can be achieved.

The parameters which were allowed to vary in the fitting procedure are: products $g_{\sigma NN}g^{(s)}_{\sigma\pi\pi}$, $g_{\sigma NN}g^{(v)}_{\sigma\pi\pi}$, and $g_{\rho NN}g_{\rho\pi\pi}$ as well as δ for the t-channel σ and ρ exchanges, $m^{(0)}_\Delta$, $g^{(0)}_{\pi N\Delta}$, and Z for the Δ mechanism, and the cut-off parameters Λ_α of the form factors given in Eq. (32). The experimental πN phase shifts were well described up to pion laboratory energies of 400 MeV. The resulting parameters and predicted phase shifts can be found in Ref. [53].

B. DMT meson-exchange model including ηN channel and higher resonances

As the energy gets higher, channels like σN, ηN, $\pi\Delta$, and ρN as well as non-resonant continuum of $\pi\pi N$ states become increasingly important, and at the same time more and more nucleon resonances appear as intermediate

states. For simplicity, we only include the ηN channel, while enlarging the Hilbert space to accommodate as many resonances as would be required by the data. We assume that each contributing bare resonance R acquires a width by coupling to πN and ηN channels.

The full t-matrix can then be written as a system of coupled equations,

$$t_{ij}(W) = v_{ij}(W) + \sum_k v_{ik}(W)\, g_k(W)\, t_{kj}(W)\,, \tag{33}$$

with i and j denoting the π and η channels and W is the total c.m. energy. The potential v_{ij} is the sum of non-resonant (v^B_{ij}) and bare resonance (v^R_{ij}) terms,

$$v_{ij}(W) = v^B_{ij}(W) + v^R_{ij}(W)\,. \tag{34}$$

The non-resonant term $v^B_{\pi\pi}$ for the πN elastic channel is taken as obtained in Sec. III A. In the channels involving η, the potential $v^B_{i\eta}$ is assumed to vanish because of the small ηNN coupling [61].

The bare resonance contribution arises from excitation and decay of the resonance R. The matrix elements of the potential $v^R_{ij}(W)$ can be symbolically expressed by

$$v^R_{ij}(q,q';W) = \frac{f_i(\tilde{\Lambda}_i,q;W)\, g^{(0,R)}_i\, g^{(0,R)}_j\, f_j(\tilde{\Lambda}_j,q';W)}{W - M^{(0)}_R + \frac{i}{2}\Gamma^{2\pi}_R(W)}\,, \tag{35}$$

where $M^{(0)}_R$ denotes the mass of bare resonance R; q and q' are the pion (or eta) momenta in the initial and final states, and $g^{(0,R)}_{i/j}$ denotes the resonance vertex couplings. $\tilde{\Lambda}_i$ stands for a triple of cut-offs, $(\Lambda_N, \Lambda_R, \Lambda_\pi)$ defined in Eq. (32). In Eq. (35), we have included a phenomenological term $\Gamma^{2\pi}_R(W)$ in the resonance propagator to account for the $\pi\pi N$ decay channel. Therefore, our "bare" resonance propagator already contains a phenomenological "dressing" effect due to the coupling to the $\pi\pi N$ channel. With this prescription we assume that any further non-resonant coupling to the $\pi\pi N$ channel can be neglected. Following Refs. [62, 63] we parameterize the two-pion width by

$$\Gamma^{2\pi}_R(W) = \Gamma^{2\pi(0)}_R \left(\frac{q_{2\pi}}{q_0}\right)^{2\ell+4} \left(\frac{X_R^2 + q_0^2}{X_R^2 + q_{2\pi}^2}\right)^{\ell+2}\,, \tag{36}$$

where ℓ is the pion orbital momentum and $q_{2\pi} = q_{2\pi}(W)$ the momentum of the compound two-pion system, and $\Gamma^{2\pi(0)}_R$ and q_0, denote the two-pion width and two-pion momentum at resonance position, respectively. $\Gamma^{2\pi(0)}_R$ and X_R are considered as free parameters. Therefore, each resonance is generally described by 6 free parameters, the bare mass $M^{(0)}_R$, decay width $\Gamma^{2\pi(0)}_R$, two bare coupling constants $g^{(0,R)}_i$ and $g^{(0,R)}_j$, and two cut-off parameters Λ_R and X_R.

The generalization of the coupled-channel model to the case of N resonances with the same quantum numbers is then given by

$$v^R_{ij}(q,q';W) = \sum_{n=1}^{N} v^{R_n}_{ij}(q,q';W)\,. \tag{37}$$

The solutions of the coupled-channel equations of Eq. (33), with potentials given in Eqs. (34-36), were fitted to the experimental πN phase shifts and inelasticities by variation of the bare resonance parameters. The fit gave good agreement with the data for all channels up to the F waves and energies below 2 GeV GeV [55], except for the partial wave F_{17} [30]. The predictions of the DMT model for the resonance parameters are presented in the next section.

IV. RESULTS AND DISCUSSION

In this section we present the nucleon resonance properties as derived from the DMT model in the elastic πN channel. The listed resonances fulfill the following criteria: (i) the pole position is restricted by $M_p \leq 2$ GeV and $\Gamma_p \leq 0.4$ GeV, (ii) the residue is larger than about 1 MeV, and (iii) the branching ratio for the one-pion channel is limited by $2\,|r_p|/\Gamma_p \geq 10$ %. Furthermore, the pole position obtained by the regularization method (RM) has to be stable over a range of derivatives (N values). In our previous work [30] we have also listed pole parameters for resonances with pole positions outside of the above restrictions. Most of these pole positions have large imaginary parts and, therefore, the RM does not converge to the analytically determined values in an acceptable way. However, if this method – based on data at physical energies – fails to predict the pole positions, it is also doubtful whether the analytic continuation of the model leads to physically significant pole positions. We may therefore assume that pole parameters outside of the discussed restrictions are not strongly supported by experimental data.

In the following tables and figures, we compare the exact resonance properties, as obtained by analytic continuation of the DMT model to the pole position, with (i) the results obtained by the speed plot and the regularization method as well as (ii) the values listed by PDG.

A. S waves

As reported in Ref. [54], we need four S_{11} resonances to fit the πN scattering amplitude in this channel, instead of only three resonances listed by PDG [13]. The additional resonance $S_{11}(1880)$ was found to play an important role in pion photoproduction as well [54], but was not seen in both the $\pi N \to \eta N$ reaction and recent measurements of η photoproduction from the proton [64, 65]. However, in the analysis of Saghai *et al.* [66] on eta photoproduction a new S_{11} state of mass $M = 1707$ MeV and width $\Gamma = 222$ MeV was needed in order to get good agreement with the data.

In our analysis we find three poles below 2 GeV (see Fig. 1, left panel). The exact pole positions are shown by asterisks with a size indicating the relative strength, proportional to $|r_p|/\Gamma_p$. Furthermore, the ranges of the PDG pole values are displayed by open boxes. The first resonance $S_{11}(1535)^{****}$ is found by both SP and RM. The second state, the $S_{11}(1650)^{****}$ is somewhat better described by RM. The third S_{11} state is very weakly excited by πN scattering and not seen by SP, whereas RM finds a nearby state. In our analysis and many others as well, the S_{11} is the most problematic partial wave due to the inelastic η threshold and two overlapping resonances with large residues. Whereas the real part of the pole positions, the pole mass M_p of the 4-star resonances are exactly found, the widths Γ_p are considerably underpredicted by RM. The situation is even worse for the moduli of the residues, which show a very bad convergence with order N. Of course, the problem has been known before. A large variation among different partial wave analyses can be found in the literature, which reflects itself in the large error bars of the PDG pole parameters for the $S_{11}(1535)$ resonance. The problem can be quantitatively expressed by the closeness of nearby singularities, with distances obtained from the central values of the PDG listing. Seen from the pole position of the $S_{11}(1535)$, the nearest singularities are the η threshold and the $S_{11}(1650)$ pole at distances of 89 MeV and 145 MeV, respectively. On the other hand, the $S_{11}(1535)$ pole lies 85 MeV away from the real axis. As a consequence, the Taylor expansion of the regular function $T^{\rm reg}$ in Eq. (11) comes close to its convergence circle if we extrapolate to the real axis. Therefore, the analytical continuation into the complex plane is strongly recommended instead of

the extrapolation. Nevertheless, if the extrapolation fails, also the exact pole parameters of a model have to be taken with a grain of salt.

For the isospin 3/2 states we obtain three poles in agreement with PDG. The first one, $S_{31}(1620)^{****}$, is nicely described by SP and perfectly by RM. The position of the second pole, $S_{31}(1900)^{**}$, is similarly well seen by both SP and RM. However, the modulus of the residue is strongly underestimated.

B. P waves

For the P-wave resonances we show our results in Fig. 2. In the P_{11} partial wave the DMT predicts two poles well inside the PDG boxes. However, the second pole lies near the lower edge of the box. The resonance parameters of the Roper or $P_{11}(1440)^{****}$ are nicely reproduced by both SP and RM. The $P_{11}(1710)^{****}$ has a very weak signal in the πN channel. Although the RM yields a considerable improvement over the SP, it misses the exact pole position and the phase of the residue.

In the P_{13} partial wave we only find one pole below 2 GeV, while PDG lists two states, the $P_{13}(1720)^{****}$ with a large error bar for the imaginary part and the $P_{13}(1900)^{**}$, however, with no pole position given. Our results for the $P_{13}(1720)$ lie close to the PDG values, with the imaginary part near to the lower limit of the PDG error bar. The RM reproduces the pole parameters of the $P_{13}(1720)^{****}$ quite well.

In the isospin-3/2 partial wave, we find the pole of the $P_{31}(1910)^{****}$ slightly outside the PDG box. All the pole parameters are well described by RM.

The Delta resonance, $P_{33}(1232)^{****}$, has, of course, the largest strength of all the poles found by our analysis. The analytic pole values are well described by both the SP and RM techniques, they also agree with the PDG listing. Due to numerical instabilities in the region of the first resonance, the RM fails for higher-order derivatives, and therefore this method can not much improve on the SP result. As a result the RM values differ slightly from the parameters obtained by analytical continuation. Another weakly excited P_{33} state is found at higher energy, which can be related to the state $P_{33}(1600)^{***}$ of PDG. The pole parameters of this second state converge well within RM. The third PDG resonance shown in Fig. 2, $P_{33}(1920)^{***}$, appears at an energy above 2 GeV in the DMT model.

C. D waves

In Fig. 3 we display the poles of D-wave resonances. PDG lists three $J = 3/2$ states with isospin 1/2, $D_{13}(1520)^{****}$, $D_{13}(1700)^{***}$, and $D_{13}(2080)^{**}$, and the DMT agrees very well within the reported ranges. Except for the residue of the $D_{13}(2080)$, we find a perfect convergence of the RM for the pole positions and residues. The $D_{13}(1700)$ is a particular case, for which the SP can not find the pole, whereas the higher-order derivatives of the RM yield very precise results.

For the D_{15} partial wave we find a rather simple contour with only one resonance, $D_{15}(1675)^{****}$, below 2 GeV. There is perfect agreement among the exact DMT values, the SP and RM extrapolations as well as the PDG listings.

For the isospin-3/2 D-wave resonances, PDG reports only one 4-star resonance, the $D_{33}(1700)^{****}$. Our analytic results are well reproduced by SP and perfectly by RM. A similar agreement is also found for the $D_{35}(1930)^{***}$. Both resonances are located very close to the PDG boxes.

D. F waves

Figure 4 displays the F-wave resonances. The $F_{15}(1680)^{****}$ is the most important resonance in the 3$^{\rm rd}$ resonance region. The exact DMT pole parameters are perfectly described by SP and RM. We also find a second F_{15} state with a small residue $|r_p| \sim 1$ GeV. Because of its location close to the real axis, this state is also well described by SP and RM. In its vicinity, PDG reports the $F_{15}(2000)^{**}$ resonance, however, with no pole parameters given. In the F_{17} partial wave we can not find a resonance by our analysis, whereas PDG lists a $F_{17}(1990)^{**}$. Our result is based on the fact that the inclusion of a bare resonance in this partial wave does not significantly improve the χ^2 fit to the data. A similar conclusion was obtained in Refs. [11, 12].

For the isospin-3/2 resonances, we find two poles corresponding to the states $F_{35}(1905)^{****}$ and $F_{37}(1950)^{****}$ reported by PDG. The pole parameters of the DMT are nicely described by SP and RM for both these resonances. However, our pole positions lie significantly above the PDG bounds for the imaginary values. This disagreement is not too surprising, because the uncertainty of a pole position rises with the distance from the real axis. In conclusion, RM converges well for the F wave amplitudes, and all pole positions and residues are obtained in full agreement with the results of the analytical continuation.

V. SUMMARY AND CONCLUSION

Within our previously developed Dubna-Mainz-Taipei (DMT) dynamical model, we have investigated the pole structure of the pion-nucleon T matrix for all S, P, D, and F partial waves in the energy range up to the c.m. energy $W = 2.0$ GeV. For this purpose, the solutions of our coupled integral equations were (i) analytically continued to unphysical energies in the range $0 > {\rm Im}W \geq -200$ MeV, (ii) mapped by contour plots, and (iii) searched for poles in the regions of interest. The resulting pole positions and residues were compared to approximative solutions as obtained by the speed plot (SP), based on the first derivative of the amplitude at physical energies, and the recently developed regularization method (RM), based on higher derivatives.

The number and positions of the DMT poles, as found by a newly developed analytic continuation method, are in good agreement with the current results of the Particle Data Group (PDG) [13], all except for the S_{11} partial waves. In particular for the $S_{11}(1535)^{****}$ and $S_{11}(1650)^{****}$ resonances, the DMT model yields much smaller widths and residues than listed by PDG. Furthermore, the model predicts an additional $S_{11}(1880)$ resonance.

Let us now turn to the main issue of our work: How well can we determine a given pole structure by our knowledge of the experimental data, that is, on the basis of the scattering amplitudes for physical energies. For that purpose we use our DMT amplitudes at physical energies as interpolating functions for the single-energy partial wave amplitudes that were obtained from the experimental data. These numerically differentiable functions serve as input for the SP and RM techniques. The approximative pole positions and residues are then compared to the exact predictions of DMT, as determined by analytic continuation of the integral equations. The results for the partial waves are

summarized as follows:

S **waves:** The pole structure of the resonance $S_{11}(1535)^{****}$ is the most problematic feature of our findings. Although the RM reproduces the real parts of the pole positions (M_p), it underpredicts the widths (Γ_p) and the moduli of the residues ($|r_p|$). However, problems with this resonance appear also in many other analyses. This is clearly visible in the large uncertainties of the respective PDG values. The reason for the failure is two-fold: (i) The two four-star resonances overlap substantially and (ii) the eta threshold lies close to the first resonance. The RM is based on the convergence of the Laurent series about the pole position in order to extrapolate from the pole to the data on the real axis and vice versa. However, the extrapolation from the $S_{11}(1535)$ pole to the real axis involves energies close to the convergence circle, which is determined by the distance between pole and eta threshold. Even worse, the input for the RM are data taken at $M_p \approx 1500$ MeV, only 25 MeV above eta threshold. This threshold enters in two ways: (i) The inelasticity lowers both the pion-nucleon branching ratio and the pole residue by about 50% and (ii) the eta yields about half of the total width. Both effects are strongly energy dependent near the eta threshold and contrary to the assumption of RM, the regular part of the Laurent expansion changes rapidly as a function of energy because of the nearby eta cusp. As a consequence, there is no convergence of the RM if applied to the $S_{11}(1535)$. Already the second derivative of the amplitude yields numerical noise with regard to the pole properties. By comparison with the first resonance, the $S_{11}(1650)^{****}$ state is much better described by RM, although the values for the width and the residue are not fully satisfactory, possibly because of the mixing with the problematic $S_{11}(1535)^{****}$ resonance. In the isospin 3/2 channel, the $S_{31}(1620)^{****}$ is perfectly described, whereas the RM result for the $S_{31}(1900)^{**}$ differs in some respects from the exact solution. Of course, this weak two-star resonance is more difficult to find, and also the PDG lists large error bars for the pole parameters.

P **waves:** For most of the *P* wave resonances, RM converges well and yields rather precise pole parameters in the range of 4-6 differentiations. Only the $P_{11}(1710)^{***}$ results are somewhat problematic, which is also reflected by large error bars given by PDG. A minor irregularity is observed for the $P_{33}(1232)^{****}$. Because of some numerical instability, the RM does not converge, and therefore the SP results can not be improved.

D **and** *F* **waves:** Already the SP yields quite reasonable values in most cases, and after 4-7 differentiations RM converges to the exact values of the pole parameters. In general, these resonances are pretty isolated and threshold effects are suppressed for the higher partial waves. An interesting case is the $D_{13}(1700)^{***}$, which is not seen by SP but correctly described by RM. Furthermore, the resonance $F_{17}(1990)^{**}$ listed by PDG with a width of 260 MeV is not found by the DMT fit to the data.

We conclude that the regularization method is a reliable method to extract the pole structure from single-channel data. In the absence of full experimental knowledge about all of the channels, this method can be sequentially applied in order to determine the pole structure relevant for the experimentally known channels of a multichannel system. However, the method loses its predictive power in regions of nearby thresholds and strongly overlapping resonances. In such cases, only an analytic continuation of the model can fully determine the structure of the singularities. Of course, such a model must describe the experimental multichannel amplitudes by a "global fit" over a large energy range. On the other hand, the regularization method is also useful when it falls short because such failure signals a complicated singularity structure of the scattering amplitude.

Acknowledgment

S.S.K. wishes to acknowledge the financial support from the National Science Council and National Center for Theoretical Sciences of ROC for his visits to the Physics Department of National Taiwan University. The work of S.N.Y. is supported in part by the NSC/ROC under grant No. NSC98-2112-M002-006. We are also grateful for the support by the Deutsche Forschungsgemeinschaft through SFB 443, the joint project NSC/DFG 446 TAI113/10/0-3, and the joint Russian-German Heisenberg-Landau program.

---

[1] H.L. Anderson, E. Fermi, E.A. Long, R. Martin, and D.E. Nagle, Phys. Rev. **85**, 934 (1952).
[2] E. Fermi, H.L. Anderson, A. Lundby, D.E. Nagle, and G.B. Yodh, Phys. Rev. **85**, 935 (1952).
[3] H.L. Anderson, E. Fermi, E.A. Long, and D.E. Nagle, Phys. Rev. **85**, 936 (1952).
[4] A. Donnachie, Springer Tracts Mod. Phys. **61**, 25 (1972).
[5] A. Donnachie, Reports on Progress in Physics **36**, 695 (1973).
[6] G. Höhler, F. Kaiser, R. Koch, and E. Pietarinen, *Handbook of Pion-Nucleon Scattering* , Physics Data 12-1, FIZ Karlsruhe (1979).
[7] R. Koch and E. Pietarinen, Nucl. Phys. **A336**, 331 (1980).
[8] R.E. Cutkosky, R.E. Hendrick, J.W. Alcock, Y.A. Chao, R.G. Lipes, J.C. Sandusky and R.L. Kelly, Phys. Rev. D **20**, 2804 (1979).
[9] R.E. Cutkosky, C.P. Forsyth, R.E. Hendrick and R.L. Kelly, Phys. Rev. D **20**, 2839 (1979).
[10] R.A. Arndt, J.M. Ford, and L.D. Roper, Phys. Rev. D **32**, 1085 (1985).
[11] R.A. Arndt, W.J. Briscoe, I.I. Strakovsky, R.L. Workman, and M.M. Pavan, Phys. Rev. C **69**, 035213 (2004).
[12] R.A. Arndt, W.J. Briscoe, I.I. Strakovsky, and R.L. Workman, Phys. Rev. C **74**, 045205 (2006).
[13] C. Amsler, *et al.* (Particle Data Group), Phys. Lett. B **667**, 1 (2008) and K. Nakamura, *et al.* (Particle Data Group), J. Phys. G **37**, 075021 (2010).
[14] W.N. Cottingham, D.A. Greenwood, "An Introduction to Nuclear Physics", Cambridge University Press, Cambridge 1986 and 2001.
[15] R.H. Dalitz and R.G. Moorhouse, Proc. R. Soc. London A **318**, 279 (1970).
[16] D. Djukanovic, J. Gegelia and S. Scherer, Phys. Rev. D **76**, 037501 (2007).
[17] J. Gegelia and S. Scherer, Eur. Phys. Jour. A **44**, 425 (2010).
[18] G. Höhler, In NSTAR2001, Proceedings of the Workshop on The Physics of Excited Nucleons, ed. D. Drechsel and L. Tiator, World Scientific 2001, 185.
[19] G.F. Chew, Berkeley UCRL-16983 (1966).
[20] G. Höhler, D.E. Groom et al., Particle Data Group, Eur. Phys. Jour. **C 15**, 1 (2000).
[21] G. Höhler and A. Schulte, PiN Newslett. **7**, 94 (1992).
[22] S. Ceci, J. Stahov, A. Švarc, S. Watson, and B. Zauner, Phys. Rev. **D 77**, 116007 (2008).
[23] C. Alexandrou, Proc. of NSTAR2009, Beijing, China, 2009, arXiv:0906.4137 [hep-lat].
[24] A. Walker-Loud et al., Phys. Rev. D **79**, 054502 (2009).
[25] J. Bulava et al., arXiv:1004.5072 [hep-lat].
[26] V. Pascalutsa, M. Vanderhaeghen, and S.N. Yang, Phys. Rept. **437**, 125 (2007).
[27] M. Lüscher, Math. Phys. **105**, 153 (1986), Nucl. Phys. B **354**, 531 (1991) and Nucl. Phys. B **364**, 237 (1991).
[28] S. Aoki et al., Phys. Rev. D **76**, 094506 (2007).
[29] V. Bernard, M. Lage, U.G. Meissner and A. Rusetsky, JHEP **0808**, 024 (2008).
[30] G.Y. Chen, S.S. Kamalov, S.N. Yang, D. Drechsel, and L. Tiator, Phys. Rev. C **76**, 035206 (2007).
[31] A. Matsuyama, T. Sato, and T.-S.H. Lee, Phys. Rept. **439**, 193 (2007).
[32] B. Julia-Diaz, T.-S.H. Lee, A. Matsuyama, and T. Sato, Phys. Rev. C **76**, 065201 (2007).
[33] V. Shklyar, H. Lenske, U. Mosel, and G. Penner, Phys. Rev. C **71**, 055206 (2005).
[34] M. Döring, C. Hanhart, F. Huang, S. Krewald, and U.-G. Meißner, Nucl. Phys. **A829**, 170 (2009).
[35] T. Inoue, E. Oset and M.J. Vicente Vacas, Phys. Rev. C **65**, 035204 (2002).
[36] E.E. Kolomeitsev, M.F.M. Lutz, Phys. Lett. B **585**, 243 (2004).
[37] S.S. Kamalov, G.Y. Chen, S.N. Yang, D. Drechsel, and L. Tiator, Phys. Lett. B **522**, 27 (2001).
[38] M. Weis *et al.* [A1 Collaboration], Eur. Phys. J. A **38**, 27 (2008).
[39] D. Hornidge, Proposal MAMI-A2/6-03 and priv. comm. (2010).
[40] L. Eisenbud, Ph.D. dissertation, Princeton University 1948, (unpublished).
[41] F.T. Smith, Phys. Rev. **118**, 349 (1960).
[42] E.P. Wigner, Phys. Rev. **98**, 145 (1955).
[43] H.M. Nussenzweig, Phys. Rev. D **6**, 1534 (1972).
[44] N. Suzuki, T. Sato, and T.-S.H. Lee, Phys. Rev. C **79**, 025205 (2009).

[45] H. Haberzettl and R. Workman, Phys. Rev. C **76**, 058201 (2007).
[46] J. von Neumann, E.P. Wigner, Physik. Z. **30**, 467 (1929).
[47] S. Ceci *et al.*, Phys. Lett. **B 659**, 228 (2008).
[48] R.L. Workman, R.A. Arndt, M.W. Paris, Phys. Rev. C **79**, 038201 (2009).
[49] A. Rittenberg *et al.*, (Review of particle properties - particle data group), Rev. Mod. Phys. **43**, S97 (1971).
[50] G. Höhler in *L*andolt-Börnstein: Elastic and Charge Exchange Scattering of Elementary Particles (Springer-Verlag 1983).
[51] C.C. Lee, S.N. Yang, and T.-S.H. Lee, J. Phys. **G17**, L131(1991).
[52] C.T. Hung, S.N. Yang, and T.-S.H. Lee, J. Phys. **G20**, 1531 (1994).
[53] C.T. Hung, S.N. Yang, and T.-S.H. Lee, Phys. Rev. C **64**, 034309 (2001).
[54] G.Y. Chen, S.S. Kamalov, S.N. Yang, D. Drechsel, and L. Tiator, Nucl. Phys. A **723**, 447 (2003).
[55] SAID partial wave analysis, solution FA02, Ref. [11].
[56] S.S. Kamalov and S.N. Yang, Phys. Rev. Lett. **83**, 4494 (1999).
[57] S.S. Kamalov, S.N. Yang, D. Drechsel, O. Hanstein, and L. Tiator, Phys. Rev. C **64**, 032201(R) (2001).
[58] E.D. Cooper and B.K. Jennings, Nucl. Phys. A **483**, 601 (1988).
[59] S. Morioka and I.R. Afnan, Phys. Rev. C **26**, 1148 (1982).
[60] B.C. Pearce and I.R. Afnan, Phys. Rev. C **34**, 991 (1986).
[61] L. Tiator, C. Bennhold, and S.S. Kamalov, Nucl. Phys. A **580**, 455 (1994).
[62] A.I. L'vov, V.A. Petrun'kin, and M. Schumacher, Phys. Rev. C **55**, 359 (1997).
[63] D. Drechsel, O. Hanstein, S.S. Kamalov, and L. Tiator, Nucl. Phys. A **645**, 145 (1999).
[64] U. Thoma, Int. J. Mod. Phys. A **20**, 1568 (2005).
[65] D. Elsner *e*t al. (CBELSA), Eur. Phys. J. A **33**, 147 (2007).
[66] B. Saghai, J. Durand, B. Julia-Diaz, HE Jun, T.-S.H. Lee, and T. Sato, Chinese Physics (HEP & NP) **33**, 1175 (2009).

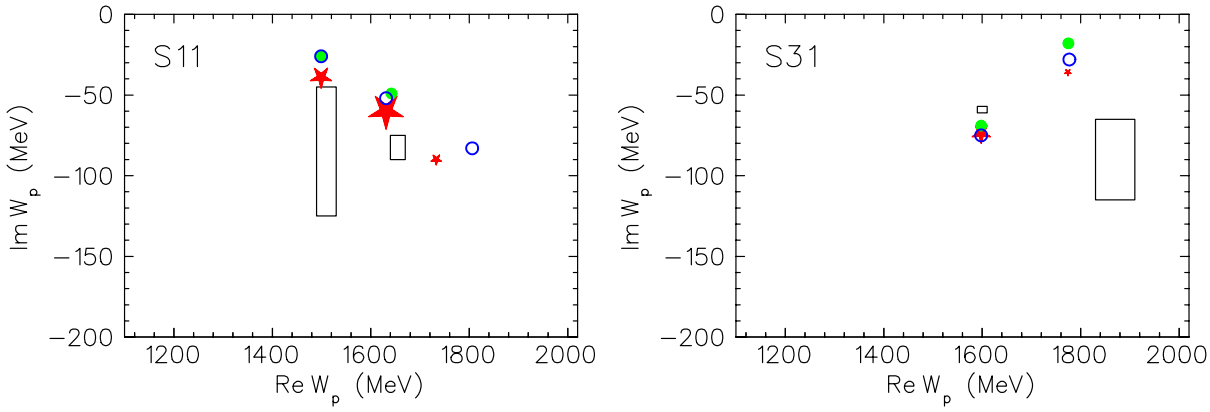

FIG. 1: The pole positions for the S waves in the complex energy plane. The (red) stars show the results found by analytic continuation, the (green) solid circles and the (blue) open circles are determined by the speed-plot and the regularization methods, respectively. The rectangular regions show the range of the pole positions listed by the Particle Data Group (PDG08) [13]. The size of the (red) stars is proportional to $|r_p|/\Gamma_p$, and therefore a measure for the strength of the resonance poles.

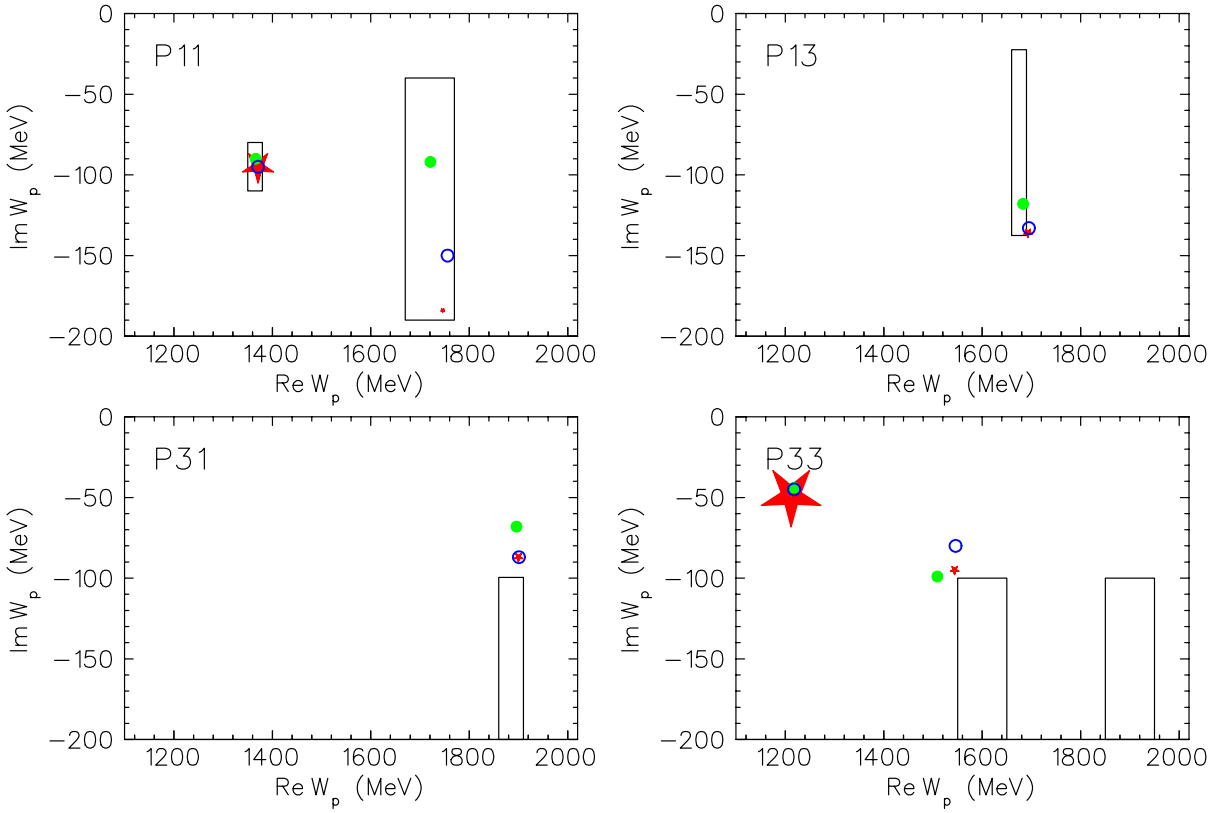

FIG. 2: The pole positions for the P waves in the complex energy plane. The notation is the same as in Fig. 1.

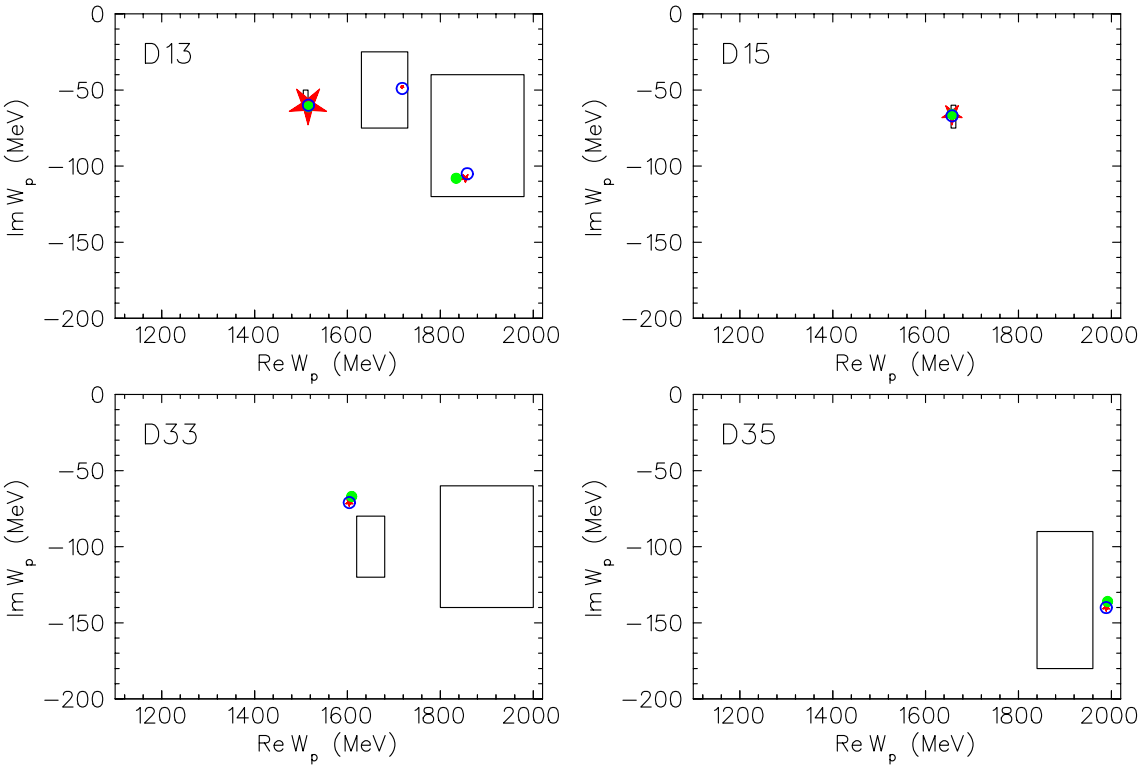

FIG. 3: The pole positions for the D waves in the complex energy plane. The notation is the same as in Fig. 1.

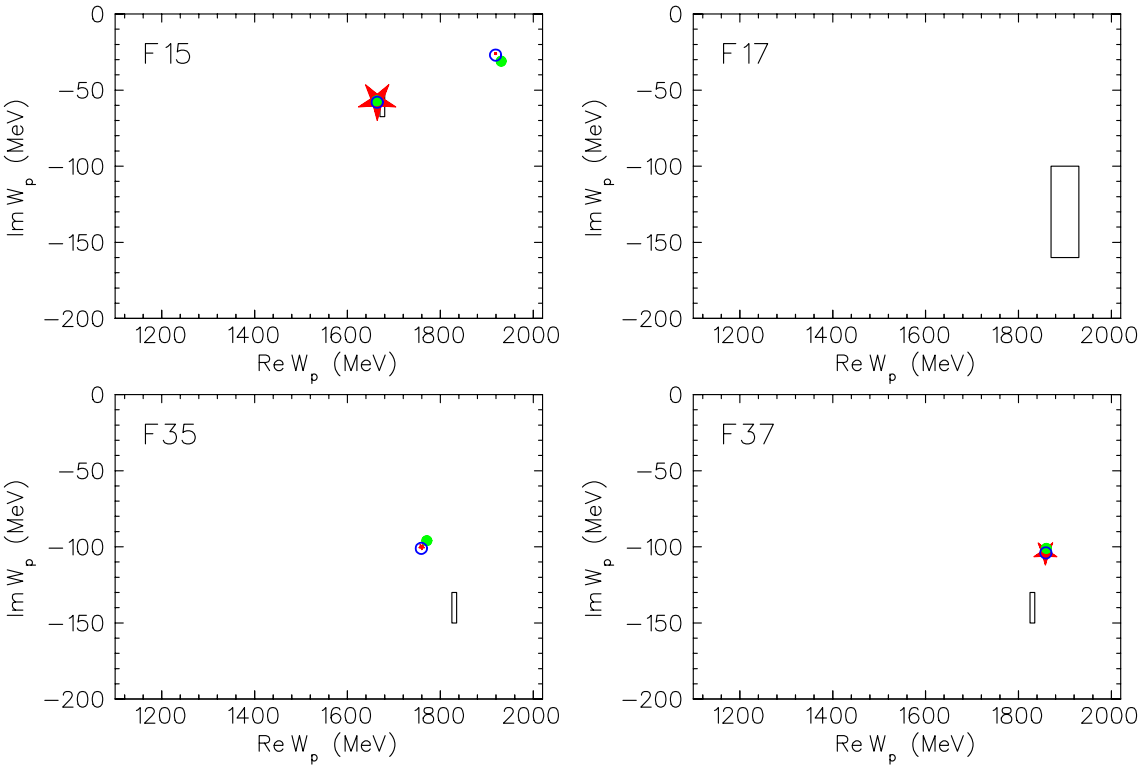

FIG. 4: The pole positions for the F waves in the complex energy plane. The notation is the same as in Fig. 1.

TABLE I: Pole positions $W_p = M_p - \frac{1}{2}i\Gamma_p$ and absolute values of the residues $\mid r_p \mid$ at the pole, all in MeV, as well as the phases θ_p of the residues for S-wave resonances. The first lines give the exact pole positions and residues as obtained by analytic continuation of the DMT model, the second and third lines show the values obtained by the speed-plot (SP) and the regularization method (RM(N)) with N being the largest value for stable derivatives. The star classification and the numerical values of the PDG are listed in the last line.

N^*	ReW_p	$-ImW_p$	$\mid r_p \mid$	θ_p(deg)
$S_{11}(1535)$	1499	39	14	-45
SP	1499	26	7	-47
RM(1)	1499	26	7	-47
****	1510 ± 20	85 ± 40	96 ± 63	15 ± 45
$S_{11}(1650)$	1631	60	35	-83
SP	1642	49	22	-74
RM(6)	1631	52	28	-119
****	1655 ± 15	83 ± 8	55 ± 15	-75 ± 25
$S_{11}(1880)$	1733	90	16	-29
SP	–	–	–	–
RM(6)	1806	83	10	-172
new				
$S_{31}(1620)$	1598	74	23	-98
SP	1598	69	23	-99
RM(6)	1598	75	24	-100
****	1600 ± 10	59 ± 2	16 ± 3	-110 ± 20
$S_{31}(1900)$	1774	36	3.8	-181
SP	1775	18	1.0	-166
RM(5)	1777	28	1	-157
**	1870 ± 40	90 ± 25	10 ± 3	-20 ± 40

TABLE II: Pole positions and residues for P-wave resonances. For further notation see Tab. I.

N^*	ReW_p	$-ImW_p$	$\mid r_p \mid$	θ_p(deg)
$P_{11}(1440)$	1371	95	50	-79
SP	1366	90	48	-87
RM(5)	1371	95	50	-78
****	1365 ± 15	95 ± 15	46 ± 10	-100 ± 35
$P_{11}(1710)$	1746	184	11	-54
SP	1721	92	5	-164
RM(6)	1756	150	11	-49
***	1720 ± 50	115 ± 75	10 ± 4	-175 ± 35
$P_{13}(1720)$	1693	136	20	-43
SP	1683	118	15	-64
RM(4)	1695	133	19	-34
****	1675 ± 15	98 ± 40	13 ± 7	-139 ± 51
$P_{31}(1910)$	1900	87	13	-116
SP	1896	68	7	-118
RM(6)	1901	87	10	-113
****	1880 ± 30	100 ± 20	20 ± 4	-90 ± 30
$P_{33}(1232)$	1212	49	49	-42
SP	1218	44	41	-35
RM(2)	1218	45	41	-35
****	1210 ± 1	50 ± 1	53 ± 2	-47 ± 1
$P_{33}(1600)$	1544	95	14	-111
SP	1509	99	25	-197
RM(5)	1546	80	11	-116
***	1600 ± 100	150 ± 50	17 ± 4	-150 ± 30

TABLE III: Pole positions and residues for D-wave resonances. For further notation see Tab. I.

N^*	ReW_p	$-ImW_p$	$\mid r_p \mid$	θ_p(deg)
$D_{13}(1520)$	1515	60	40	-7
SP	1516	61	40	-6
RM(5)	1516	60	40	-5
****	1510 ± 5	55 ± 5	35 ± 3	-10 ± 4
$D_{13}(1700)$	1718	48	2.8	-91
SP	–	–	–	–
RM(7)	1718	49	2.9	-91
***	1680 ± 50	50 ± 25	6 ± 3	0 ± 50
$D_{13}(2080)$	1854	108	16	-97
SP	1834	108	14	-134
RM(6)	1858	105	9	-83
**	1950 ± 170	100 ± 40	27 ± 22	~ 0
$D_{15}(1675)$	1657	66	24	-22
SP	1657	66	24	-23
RM(6)	1657	67	25	-22
****	1660 ± 5	68 ± 6	29 ± 6	-30 ± 10
$D_{33}(1700)$	1604	71	9.4	-63
SP	1609	67	9.5	-52
RM (6)	1604	71	9.9	-63
****	1650 ± 30	100 ± 20	13 ± 3	-20 ± 25
$D_{35}(1930)$	1989	140	18	-78
SP	1992	136	19	-75
RM(5)	1989	140	18	-78
***	1900 ± 50	133 ± 48	18 ± 6	-20 ± 40

TABLE IV: Pole positions and residues for F-wave resonances. For further notation see Tab. I.

N^*	ReW_p	$-ImW_p$	$\mid r_p \mid$	θ_p(deg)
$F_{15}(1680)$	1664	57	38	-26
SP	1663	57	38	-28
RM(6)	1664	58	39	-26
****	1672 ± 8	61 ± 6	38 ± 3	-23 ± 7
$F_{15}(2000)$	1919	26	1.0	15
SP	1931	31	1.3	89
RM(4)	1919	27	1.1	15
**	1807	54.5	60	-67
$F_{17}(1990)$	–	–	–	–
SP	–	–	–	–
RM	–	–	–	–
**	1900 ± 30	260 ± 60	9 ± 3	-60 ± 30
$F_{35}(1905)$	1760	100	10	-66
SP	1771	96	11	-47
RM(5)	1759	101	10	-66
****	1830 ± 5	140 ± 10	25 ± 8	-50 ± 20
$F_{37}(1950)$	1858	104	43	-48
SP	1860	101	44	-45
RM(5)	1859	104	44	-47
****	1880 ± 10	140 ± 10	50 ± 7	-33 ± 8